A SIMPLE AND GENERAL SUBGRID MODEL SUITABLE BOTH FOR SURFACE LAYER AND FREE-STREAM TURBULENCE

J. L. REDELSPERGER[1,2], F. MAHÉ[1] and P. CARLOTTI[2,3]
[1]*ONERA, 29 Avenue de la Division Leclerc, 92320 Chatillon, France;* [2]*Centre National de Recherches Météorologiques, CNRS & Météo-France, 42 Avenue G. Coriolis, 31057 Toulouse Cedex 1, France;* [3]*Department of Applied Mathematics and Theoretical Physics, University of Cambridge, Silver Street, Cambridge CB3 9EW, U.K.*

(Received in final form 10 April 2001)

Abstract. A new and general approach is presented to allow standard subgrid schemes to be suitable both for surface layer and free-stream turbulence. Simple modifications to subgrid schemes are proposed and derived for any vertical stability conditions. They are simple to implement in models and are suitable for more complicated simulations such as large-eddy simulation with inhomogeneous surface conditions or complex topography. They are also applicable to mesoscale and large-scale models. These modifications are physically justified by recent measurements of spectra close to the ground. The spectral analysis presented shows how the energy deficit of blocked turbulence for a given dissipation ('anomalous dissipation') dramatically affects the coefficients to be used in subgrid schemes. As shown for neutral and convective cases with wind shear, these changes allow us to substantially improve the prediction of profiles for the mean quantities in the surface layer. Agreement with similarity laws in the unstable case is found up to about $0.2z_i$, for simulated shear, stability profiles and dissipation rates of turbulent kinetic energy.

Keywords: Boundary layer, LES, Similarity, Subgrid scale schemes, Surface layer.

1. Introduction

The representation of the full depth of the atmospheric boundary layer with a unique parameterization is a difficulty shared by all numerical models from large-eddy simulations (LES) to general circulation models. This issue has been considered in numerous works, mostly in the LES context. The purpose of the present paper is to provide a physical explanation and a solution suitable for any models. LES are now widely used as powerful tools to study various turbulent flows occuring in the planetary boundary layer (PBL). Large eddy simulation models separate the scales of turbulence into two ranges, resolved and subgrid scales. The resolved scales (representing larger scales) are assumed to contain most of the energy of turbulent motion whilst on subgrid scales, motions are the less energetic. This approach works well far from regions of large gradients. In the mid-PBL, for example, the resolved vertical fluxes are on average about 10 times larger than the subgrid vertical fluxes. However, results from LES show that the subgrid contribu-

Boundary-Layer Meteorology **101:** 375–408, 2001.

tion becomes larger than the resolved part near the surface or where temperature inversions exist. In this paper, we will only address the first of these two issues.

The horizontal characteristic size of energy-containing eddies scales with distance from the surface (for a review, see Counihan, 1975). As an immediate consequence, LES fails to explicitly resolve these eddies. Turbulence near the surface is thus mostly taken into account through the subgrid-scale parameterisation. Consequently, LES results become more sensitive to the subgrid scheme in this region. Past studies (Mason and Thomson, 1992; Andrèn et al., 1994; Sullivan et al., 1994) have shown that the traditional subgrid-scale eddy viscosity fails to predict the shear profile near the surface. It is a long-standing problem in LES that the wind profile differs from similarity laws in the surface layer. Moin and Kim (1982) had previously shown for LES of shear-driven channel flow that the turbulence cannot be maintained without decreasing the energy dissipation. In general the mean shear is over-predicted near the ground in standard LES. This error can contaminate the solution in the whole atmospheric boundary layer through buoyancy driven vertical fluxes (Khanna and Brasseur, 1998). Using direct numerical simulations, Juneja and Brasseur (1999) have diagnosed several shortcomings in current subgrid turbulence schemes mainly linked to the neglected acceleration terms.

To better predict the gradients of wind and temperature in the near-surface region, Mason and Thomson (1992) and Sullivan et al. (1994) suggested modifications to subgrid turbulence schemes. Their models show improved prediction of the main characteristics in the surface layer. Mason and Thomson (1992) argued that the local energy transfer from subgrid to resolved scales can become important when the more energetic scales are not resolved. They included a stochastic 'backscatter' of energy to represent this transfer leading to an empirical increase in the Smagorinsky constant when approaching the wall. Sullivan et al., (1994) (hereafter SWM94) modified their subgrid scheme by forcing the subgrid stresses to approach the mean resolved turbulent stresses near the surface. In other words, the subgrid viscosity is adapted so that the similarity law is strictly verified at the first model level and with a relaxation above. These modifications appear to work in the near neutral boundary layer. LES have also been performed through the use of dynamical models as proposed by Germano et al. (1991). In relating stresses at different scales, the subgrid-scale coefficient is determined from the resolved scales and is assumed scale invariant. This formulation of the dynamical models breaks down near a rigid boundary. A generalization of the dynamical model, which allows the coefficient to change with the mesh size in a consistent manner, was recently suggested by Porté-Angel et al. (2000). This latter approach was found to largely improve the results near the surface as given in LES of neutral atmospheric boundary layers. It is worthwhile to notice that in all the approaches summarized above, the subgrid mixing length is assumed to be the Prandtl mixing length κz near the wall.

Khanna and Brasseur (1997) have examined in detail how well high-resolution LES predicts means, variances, budgets of turbulent kinetic energy and temperat-

ure variance, compared with observed Monin–Obukhov similarity laws. Horizontal and vertical resolutions are also important issues to consider though it is impractical to have enough resolution to solve all energetic motions in the whole surface layer. Clearly, the better the resolution, the larger is the well simulated part of the surface layer. Nevertheless, Khanna and Brasseur (1997) have shown that the improvement to expect from a modified subgrid scheme is much better than the improvement gained from an increase of resolution. In this paper, we will use horizontal and vertical resolutions currently used in standard LES.

The present study seeks a simple approach to improve the representation of the surface layer in standard LES. The approach is also required to be suitable for more complicated models such as LES with inhomogeneous surface conditions, complex topography and any vertical stability conditions. In a further paper, an application of the same method to mesoscale and large-scale models will be presented. Section 2 presents the general problem of applicability to surface-layer behaviour of standard subgrid schemes designed to work in free-stream turbulence. Section 3 uses some recent results on spectra near the surface to give the physical basis of our approach; this spectral analysis discards for the choice of the subgrid mixing length the Prandtl mixing length κz. The resulting subgrid model is proposed in Section 4. The idea is to have a scheme for the above specified conditions including applications to mesoscale and large-scale models. Results from LES using this approach are shown in Section 5, together with comparisons with observations and previous LES studies. Mean wind and temperature profiles as well as other statistical moments are compared to observed Monin–Obukhov similarity laws fitted on observations.

2. The Problem

In atmospheric boundary-layer modelling it is standard practice to look at the behaviour of turbulence closures in considering the one-dimensional, neutrally stratified case. This simple case is enough to illustrate the general problem of reliability of subgrid turbulence scheme derived for free sheared turbulence when applied to turbulence blocked by a 'wall'.

Using the equilibrium theory for an horizontally homogeneous turbulent flow (e.g., Townsend, 1976, pp. 135–140), the turbulent kinetic energy equation reduces to a balance of dissipation ε with shear production:

$$\varepsilon = -\overline{u'w'}\frac{\partial \overline{u}}{\partial z} - \overline{v'w'}\frac{\partial \overline{v}}{\partial z} \tag{1}$$

where u, v, w are the components of wind along x, y, and z directions, respectively (z is the vertical direction, perpendicular to the ground).

In the common subgrid-scale eddy viscosity approach, the Reynolds stresses are modelled as:

$$-\overline{u'w'} = K_m \frac{\partial \overline{u}}{\partial z} \tag{2}$$

$$-\overline{v'w'} = K_m \frac{\partial \overline{v}}{\partial z} \tag{3}$$

with

$$K_m = \mathcal{L}_{\mathcal{K}} E^{1/2}, \tag{4}$$

where E denotes the subgrid turbulent kinetic energy and $\mathcal{L}_{\mathcal{K}}$ has the dimension of a length.

Dimensional arguments show that the dissipation can be expressed as

$$\varepsilon = \frac{E^{3/2}}{\mathcal{L}_\varepsilon}, \tag{5}$$

where $\mathcal{L}_\varepsilon$ has the dimension of a length.

In mesoscale and large-scale models, the lengths are generally specified using empirical formulations (e.g., Louis, 1979) or by using the properties of the boundary layer in the considered column of the atmosphere (e.g., Troen and Mahrt, 1986; Cuxart et al., 2000).

In LES models, for the case of free turbulence (i.e., away from the ground), spectral arguments can be used (e.g., Schmidt and Schumann, 1989, see also Section 3) to show that:

$$\mathcal{L}_{\mathcal{K}} = C_K L \tag{6}$$

$$\mathcal{L}_\varepsilon = \frac{L}{C_\varepsilon} \tag{7}$$

where L is the mesh size and

$$C_\varepsilon = \pi \left(\frac{2}{3\alpha_3} \right)^{\frac{3}{2}} \tag{8}$$

$$C_K = \frac{1}{\pi} \left(\frac{2}{3\alpha_3} \right)^{\frac{3}{2}} \tag{9}$$

where α_3 is the 'three-dimensional' Kolmogorov constant. Measurements give $\alpha_3 = 1.6 \pm 0.02$ (Andreas, 1987).

In some LES models (e.g., SWM94), this unique length scale L is bounded near the surface to κz, where κ is the Von Karman constant, but there is no clear theoretical justification for this assumption. The goal of the following is to derive some theoretical arguments for the values of $\mathcal{L}_{\mathcal{K}}$ and $\mathcal{L}_\varepsilon$ close to the ground.

Using the equilibrium hypothesis (Equation (1) together with Equations (2)–(5)), the subgrid turbulent kinetic energy and the Reynolds stress can be written as:

$$E = \mathcal{L}_\varepsilon \mathcal{L}_\mathcal{K} \left[\left(\frac{\partial \overline{u}}{\partial z} \right)^2 + \left(\frac{\partial \overline{v}}{\partial z} \right)^2 \right] \tag{10}$$

$$\overline{u'w'}^2 + \overline{v'w'}^2 = \mathcal{L}_\mathcal{K}{}^3 \mathcal{L}_\varepsilon \left[\left(\frac{\partial \overline{u}}{\partial z} \right)^2 + \left(\frac{\partial \overline{v}}{\partial z} \right)^2 \right]^2 \tag{11}$$

On the other hand, the similarity theory for the surface layer allows in the neutral case to relate the wind-speed gradient to the friction velocity u_* through

$$\frac{u_*}{\kappa z} = \left[\left(\frac{\partial \overline{u}}{\partial z} \right)^2 + \left(\frac{\partial \overline{v}}{\partial z} \right)^2 \right]^{\frac{1}{2}} \tag{12}$$

$$E = \alpha {u_*}^2 \tag{13}$$

where ${u_*}^2 = \left(\overline{u'w'}|_{sfc}{}^2 + \overline{v'w'}|_{sfc}{}^2 \right)^{\frac{1}{2}}$, κ is the Karman constant, and subscript $|_{sfc}$ indicates surface value. Observational data suggest α ranges from 3.75 (Wyngaard et al., 1974) to 5.47 (Garratt, 1992).

In order to compare these relationships to those derived from the turbulence subgrid parameterisation, they can be rewritten as:

$$E = \alpha \kappa^2 z^2 \left[\left(\frac{\partial \overline{u}}{\partial z} \right)^2 + \left(\frac{\partial \overline{v}}{\partial z} \right)^2 \right] \tag{14}$$

$$\overline{u'w'}^2 + \overline{v'w'}^2 = (\kappa z)^4 \left[\left(\frac{\partial \overline{u}}{\partial z} \right)^2 + \left(\frac{\partial \overline{v}}{\partial z} \right)^2 \right]^2. \tag{15}$$

So far, the equations for the subgrid scheme ((10), (11)) and for the similarity laws ((14), (15)) have been derived separately. Now supposing that both are valid in the surface layer, the two following equations are obtained:

$$\mathcal{L}_\mathcal{K} = \frac{1}{\sqrt{\alpha}} \kappa z \tag{16}$$

$$\mathcal{L}_\varepsilon = \alpha^{\frac{3}{2}} \kappa z. \tag{17}$$

Going back to the more conventional notations (6) and (7), it can be finally written:

$$L = \kappa z \tag{18}$$

$$C_\varepsilon|_{sfc} = \frac{1}{\alpha^{\frac{3}{2}}} \tag{19}$$

$$C_K|_{sfc} = \frac{1}{\sqrt{\alpha}}. \tag{20}$$

For $\alpha = 3.75$ (5.47), we should have for the neutral surface layer

$$C_\varepsilon|_{sfc} = 0.137\ (0.078) \tag{21}$$

$$C_K|_{sfc} = 0.516\ (0.428). \tag{22}$$

In fact, the constants in the subgrid turbulence schemes are kept to their free-stream values ((8), (9)), (9)) as discussed above. In the present model, the values of C_ε and C_K are thus 0.7 and 0.066, respectively. In the following, C_K and C_ε are used exclusively for these free-stream values.

For cases where the primary balance is between shear production and dissipation, these free-stream values imply in the surface layer a value of the turbulent kinetic energy that is too small and a vertical wind shear that is too large. This shortcoming of current subgrid turbulence schemes is illustrated in Figure 1 showing a comparison between LES and similarity theory predictions for a neutral case. It is important to notice that the problem does not originate from a bad choice of constants but from the use in the surface layer of a subgrid scheme derived for free-stream turbulence. Two main hypotheses, used to derive the subgrid fluxes given by Equations (10) and (11) from the full second-order moment equations, seem to fail especially in the surface layer. First, as discussed in Sommeria (1976), Mason and Thomson (1992), and Cuxart et al. (2000), it is assumed that turbulence is isotropic. Near the surface, the anisotropic production rates clearly become important. Second, it is hypothesised that the mesh size lays inside the inertial range of the energy spectrum. This hypothesis is not relevant near the surface where energy-containing eddies scale roughly with the distance from the surface (Counihan, 1975). It is therefore not surprising that the standard subgrid schemes cannot be applied in a straightforward manner to LES models near the surface. This remark, made for LES models, can also be applied to 1D turbulence schemes such as those used in mesoscale and general circulation models (GCM). The simple derivation above gives a simple explanation as to why the constant C_K used in these latter models is generally set up empirically to values larger than 0.066. For mesoscale and large-scale models, Therry and Lacarrere (1983), for example, proposed a value as large as $C_K = 0.5$.

For LES models, two types of solutions to this problem have been proposed. Firstly, larger values of the constants $C_\varepsilon|_{sfc}$ and $C_K|_{sfc}$ can be empirically specified as in some mesoscale and large-scale models. The drawback is that these values

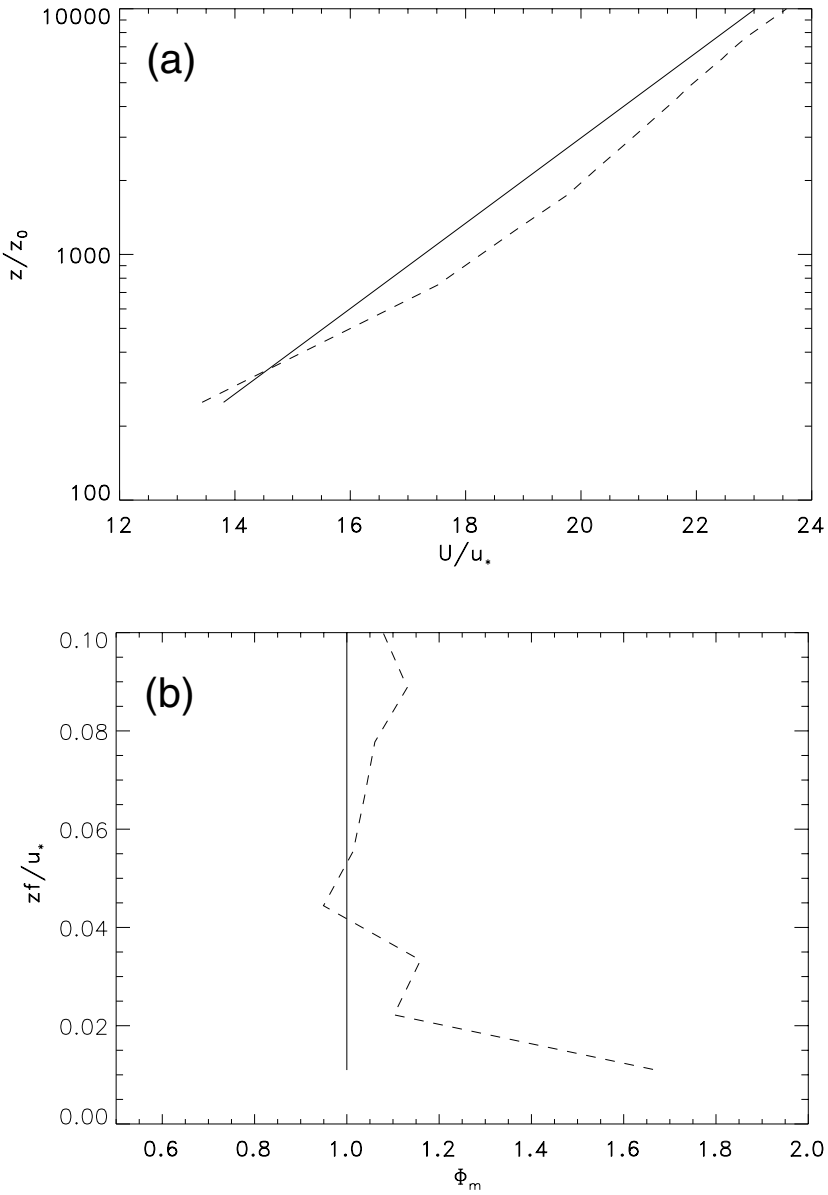

Figure 1. Profiles for neutral flow of (a) normalized wind speed and (b) vertical shear as computed from standard LES (dashed line) and deduced from similarity theory (solid line).

are no longer adapted to free-stream turbulence where they should be determined as described above. Secondly, we can make the subgrid turbulence scheme more complex by introducing an anisotropic term that becomes larger near the surface (e.g., Schumann, 1975; Moin and Kim, 1982; Mason and Thomson, 1992; SWM94). This last method has shown to be efficient in improving the simulation of the surface layer in LES. The present study seeks a method simple to implement and suitable for LES models as well as mesoscale models and GCMs. In particular, we want the method to be applicable for any stability conditions and any type of surface (e.g., over complex topography or heterogeneous roughness).

3. Spectral Analysis of the Problem

3.1. Introduction

Away from the ground, one usually considers the three-dimensional spectrum $E(k)$, which represents the turbulent kinetic energy, within the range of wave numbers $[k, k + \mathrm{d}k]$. Close to the ground, one cannot consider the turbulence to be nearly isotropic, and therefore one must be more careful with the definitions. Writing u_i for the fluctuating velocity field, one can define $R_{ij}(r, z) = \langle u_i(x, y, z)u_j(x + r, y, z)\rangle$ where $\langle\ .\ \rangle$ is the ensemble average. Then, we denote by $E_{ij}(k_1, z)$ the Fourier transform of R_{ij} with respect to r and $E(k_1, z) = \frac{1}{2}(E_{11}(k_1, z) + E_{22}(k_1, z) + E_{33}(k_1, z))$. Obviously, the turbulent kinetic energy at the height z is given by $\int_{-\infty}^{+\infty} E(k_1, z)\,\mathrm{d}k_1$.

Some recent measurements have shown that these velocity spectra change dramatically close to the ground (cf. Hoxey and Richards, 1992; Kim and Adrian, 1999; Fuehrer and Friehe, 1999) in the following way: for $k_1 > 2\pi/z$, E_{11}, E_{22} and E_{33} behave in the same ways as in homogeneous turbulence, but for $2\pi/\Lambda < k_1 < 2\pi/z$, where Λ is a very large length scale (up to 12 times the boundary-layer height or the pipe radius in pipe experiments), E_{11} and E_{22} have a self similar behaviour in k_1^{-1} while E_{33} is roughly flat (see Figure 2). This behaviour is analysed from a theoretical point of view in Hunt and Morrison (2000) and Hunt and Carlotti (2000).

This gives the following approximate behaviour for $E(k_1)$:

$$E(k_1) = \begin{cases} \frac{3}{10}\alpha_3\varepsilon^{2/3}k_1^{-5/3} & \text{if} \quad k_1 > 2\pi/z \\ \frac{6}{55}\alpha_3\varepsilon^{2/3}\frac{z^{2/3}}{(2\pi)^{2/3}}[\frac{21}{12}\frac{1}{k_1} + \frac{z}{2\pi}] & \text{if} \quad 2\pi/z > k_1 > 2\pi/\Lambda \end{cases} \tag{23}$$

with $\varepsilon(z) = u_*^3/(\kappa z)$. In homogeneous isotropic turbulence, one simply has $E_{\mathrm{hom}} = \frac{3}{10}\alpha_3\varepsilon^{2/3}k_1^{-5/3}$ for all k.

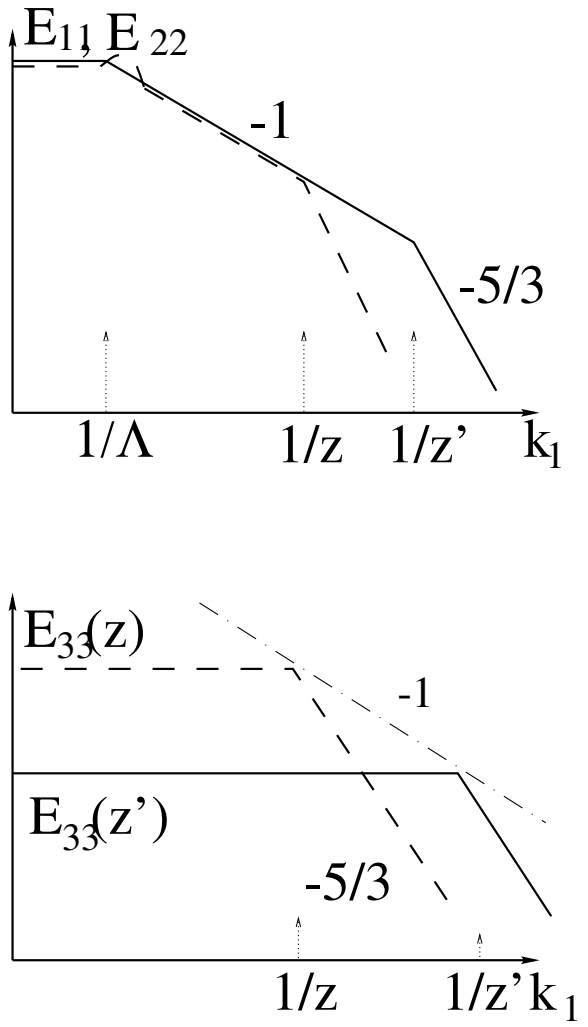

Figure 2. Sketch of the measured one-dimensional spectra in atmosphere and pipe very close to the boundary (cf. Hunt and Carlotti (2000) for most details about these spectra).

3.2. DISSIPATION LENGTH SCALE

This form of the spectra produces a deficit of turbulent kinetic energy for a given dissipation, as indicated by the shaded area in Figure 3.

More precisely, first we recall the method described in Schmidt and Schumman (1989) for homogeneous turbulence. Knowing that $E_{\text{hom}}(k) = \alpha_3 \varepsilon^{2/3} k^{-5/3}$, one can calculate E_{hom} the subgrid kinetic energy by

$$E_{\text{hom}} = \int_{k_H}^{\infty} E_{\text{hom}}(k)\,\mathrm{d}k = \frac{3\alpha_3}{2} \varepsilon^{2/3} k_H^{-2/3}. \tag{24}$$

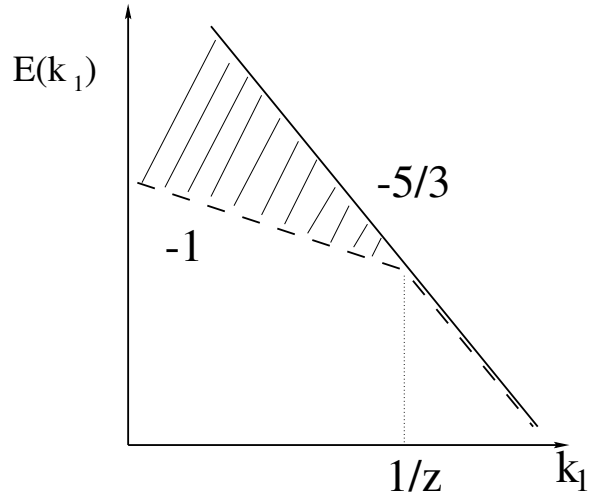

Figure 3. Illustration of the anomalous dissipation close to a surface: solid line (——): one-dimensional kinetic energy spectrum for isotropic turbulence for a given dissipation; dashed line (– – –): one-dimensional kinetic energy for wall blocked turbulence and the same dissipation.

Now, if Δ is the mesh size, one finds $k_H = \pi/\Delta$, where k_H is the cut-off wavenumber of the filter. Therefore one gets

$$\mathcal{L}_\varepsilon = \frac{\Delta}{\pi[2/(3\alpha_3)]^{3/2}} \tag{25}$$

or

$$\mathcal{L}_\varepsilon = \frac{L}{C_\varepsilon} \quad \text{with} \quad C_\varepsilon = \pi\left(\frac{2}{3\alpha_3}\right)^{3/2}. \tag{26}$$

In the case of turbulence blocked by the ground, having a behaviour as shown in Figure 2, a completely rigourous argument is not possible any more, because there is no clear definition of what the large eddies are. However, as it can be seen in Figure 3, for a given dissipation, there is a deficit of turbulent kinetic energy in the case of wall-bounded turbulence. Define

$$\Xi_\varepsilon = \frac{\int_{k_H}^{\infty} E_{\text{hom}}(k_1)\,\mathrm{d}k_1}{\int_{k_H}^{\infty} E_{bl}(k_1)\,\mathrm{d}k_1}, \tag{27}$$

where E_{bl} is given by Equation (23). We claim that Ξ_ε, which is defined with respect to the streamwise direction, is a good measure of the global deficit of turbulent kinetic energy; the turbulent kinetic energy of the actual flow is equal to E_{hom} (given by Equation (24)) divided by Ξ_ε,

$$E = \frac{E_{\text{hom}}}{\Xi_\varepsilon} \quad \Rightarrow \quad \varepsilon = C_\varepsilon \frac{E^{3/2}}{\Delta/\Xi_\varepsilon^{3/2}}. \tag{28}$$

Using Equation (23) and its equivalent for homogeneous turbulence, it is straightforward to calculate

$$\Xi_\varepsilon = \frac{(2\Delta/z)^{2/3}}{7/22\ln(2\Delta/z) + 2/11(1 - z/(2\Delta)) + 1}. \tag{29}$$

Taking Equations (28) and (29), one therefore gets

$$\varepsilon = C_\varepsilon \frac{E^{3/2}}{A_\varepsilon z} \quad \text{where } A_\varepsilon = \frac{1}{2}\Big(\frac{7}{22}\ln\frac{2\Delta}{z} + \frac{2}{11}\Big(1 - \frac{z}{2\Delta}\Big) + 1\Big)^{3/2}. \tag{30}$$

3.3. Eddy viscosity length scale

Evaluating $\mathcal{L}_\mathcal{K}$ is even less easy to do rigourously. For simplicity, we will therefore first show the case of free-stream turbulence, using the same arguments as Schmidt and Schumman (1989) but a different mathematical formulation, and only after that deal with wall-bounded turbulence.

First, we recall Equation (1) ($\overline{(.)}$ denotes the filtering operation)

$$\varepsilon = -\overline{u'w'}\frac{\partial\overline{u}}{\partial z} - \overline{v'w'}\frac{\partial\overline{v}}{\partial z}.$$

Used together with Equations (2) and (3), this gives

$$\varepsilon = K_m[(\partial_z\overline{u})^2 + (\partial_z\overline{v})^2]. \tag{31}$$

Now, using a three-dimensional Fourier transform, we know that

$$\underline{u}(\underline{x}) = \iiint \underline{\hat{u}}(\underline{k})e^{i\underline{k}.\underline{x}}\,\mathrm{d}\underline{k}$$

and therefore, writing $\hat{H}$ for the filter in the spectral space,

$$\overline{\underline{u}}(\underline{x}) = \iiint \hat{H}(\underline{k})\underline{\hat{u}}(\underline{k})e^{i\underline{k}.\underline{x}}\,\mathrm{d}\underline{k} \text{ and } \partial_z\overline{u_i} = \iiint ik_z\hat{H}(\underline{k})\underline{\hat{u}_i}(\underline{k})e^{i\underline{k}.\underline{x}}\,\mathrm{d}\underline{k}.$$

Therefore, using the dagger (†) to denote the complex conjugate,

$$\begin{aligned}\langle\partial_z\overline{u_i}\partial_z\overline{u_j}\rangle &= \left\langle \iiint\iiint\iiint k_z k_z'\hat{H}(\underline{k})\hat{H}(\underline{k}')^\dagger\underline{\hat{u}_i}(\underline{k})\underline{\hat{u}_i}(\underline{k}')^\dagger e^{i(\underline{k}-\underline{k}').\underline{x}}\,\mathrm{d}\underline{k}\,\mathrm{d}\underline{k}'\right\rangle \\ &= \iiint k_z^2\hat{H}(\underline{k})\Phi_{ij}(k_x,k_y,k_z)\,\mathrm{d}k_x\,\mathrm{d}k_y\,\mathrm{d}k_z,\end{aligned}$$

where $\langle\ .\ \rangle$ denotes an ensemble average, Φ_{ij} is the three-dimensional spectral correlation tensor and use has been made of the Wiener–Khintchine Theorem (H

is assumed to be a top-hat filter, so that $\hat{H}^2 = \hat{H}$). Now, the ensemble-averaged velocity is independent of x and y, and its vertical component is 0. Therefore

$$\begin{aligned}\langle(\partial_z\overline{u})^2 + (\partial_z\overline{v})^2\rangle &= \sum_{i,j}\langle(\partial_{x_i}\overline{u_j})^2\rangle \\ &= \iiint_{(k<k_H)} k^2(\Phi_{11}+\Phi_{22}+\Phi_{33})\mathrm{d}k_x\mathrm{d}k_y\mathrm{d}k_z \\ &= 2\int_0^{k_H} k^2 E(k)\mathrm{d}k.\end{aligned}$$

Going back to Equation (31), we get

$$\langle\varepsilon\rangle = 2K_m\int_0^{k_H} k^2E(k)\mathrm{d}k. \tag{32}$$

Now, due to the k^2 term in the integral, the very large eddies contribute very little to it. The main contribution comes from the inertial range if k_H is larger than that at the beginning of the inertial range. In the case of free-stream turbulence, it is then straightforward to obtain

$$\langle\varepsilon\rangle = 2K_m\frac{3\alpha_3}{4}\langle\varepsilon\rangle^{2/3}(\pi/\Delta)^{4/3}$$

and therefore, using Equation (5),

$$K_m = \frac{2}{3\alpha_3}\frac{E^{1/2}}{\varepsilon^{1/3}}(\Delta/\pi)^{4/3}. \tag{33}$$

Then using the free-stream value for $\mathcal{L}_\varepsilon = \Delta/C_\varepsilon$ and writing $K_m = C_K\Delta E^{1/2}$, one can get the value of C_K given in Equation (9) for the case of free-stream turbulence.

In the case of turbulence blocked by a surface, as noticed already for the evaluation of the dissipation scale, it is not possible to use three-dimensional Fourier transforms. We will therefore use the same level of approximation as for the dissipation scale, writing

$$\langle(\partial_z\overline{u})^2 + (\partial_z\overline{v})^2\rangle = \frac{2}{\Xi_K}\int_0^{k_H} k^2E_{\mathrm{hom}}(k)\,\mathrm{d}k, \tag{34}$$

where

$$\Xi_K = \frac{\int_0^{k_H} k_1^2E_{\mathrm{hom}}(k_1)\,\mathrm{d}k_1}{\int_0^{k_H} k_1^2E_{bl}(k_1)\,\mathrm{d}k_1} \tag{35}$$

and therefore

$$K_m = \frac{2}{3\alpha_3 \Xi_K} \frac{E^{1/2}}{\mathcal{L}_\varepsilon^{1/3}} (\Delta/\pi)^{4/3}. \tag{36}$$

Using the form of the spectrum shown in Figure 2, one gets, using $k_H = \pi/\Delta$,

$$\Xi_K = \frac{33/16}{(z/2\Delta)^{2/3}[(7/8) + (1/3)(z/2\Delta)]}. \tag{37}$$

Noticing that $C_K = (2/3\alpha_3) C_\varepsilon^{1/3}/\pi^{4/3}$, we can use the notation

$$\mathcal{L}_\mathcal{K} = C_K A_K z \quad \text{where } A_K = \frac{\Xi_\varepsilon^{1/2}}{\Xi_K} \frac{\Delta}{z} \tag{38}$$

and therefore

$$A_K = \frac{7 + (8/3)(z/2\Delta)}{33\sqrt{(7/22)\ln 2\Delta/z + (2/11)(1 - z/(2\Delta)) + 1}} \left(\frac{2\Delta}{z}\right)^{2/3}. \tag{39}$$

3.4. Discussion of these results

The values of A_K and A_ε are plotted on Figure 4. It can be seen that, for $z = 2\Delta$, $\mathcal{L}_\mathcal{K}/C_K \approx C_\varepsilon \mathcal{L}_\varepsilon \approx \Delta$, and that both A_K and A_ε tend to large values when $z/\Delta \to 0$. Note that the models (e.g., SWM94), where it is assumed that $\mathcal{L}_\mathcal{K}/C_K = C_\varepsilon \mathcal{L}_\varepsilon = \text{Min}(\Delta, \kappa z)$, are discarded by our analysis. This corresponds to assuming that $A_\varepsilon = A_K = 0.4$ close to the ground, which is far too small. Our new values do not violate any physical consideration, since the Karman constant arises from consideration of a single length scale close to the ground, which is not correct in choosing the subgrid model of LES, where the filter characteristic length is relevant in all the domain of computation.

The calculations shown in this section have been made using many approximations, especially for the blocked case, where Ξ_K and Ξ_ε are assumed to represent the blocking, and where the top-hat property of the filter is used for the eddy-viscosity length. These assumptions mean that we can be confident in the predicted values of A_ε and A_K, up to a multiplicative coefficient of order one.

On a more theoretical point of view, the main result of this spectral analysis is to show how the energy deficit of blocked turbulence for a given dissipation (this can be called 'anomalous dissipation') has a dramatic effect on the coefficients to be used in large eddy simulation close to the ground, causing A_ε and A_K to become large ($A_K \propto z^{-2/3}$, $A_\varepsilon \propto (\ln 1/z)^{3/2}$). It must be kept in mind that the k_1^{-1} range in the spectrum appears only at relatively large Reynolds numbers, when the thickness of the viscous sublayer and the roughness sublayer are small compared with all the other lengths. It is always the case in the atmospheric boundary layer, where the

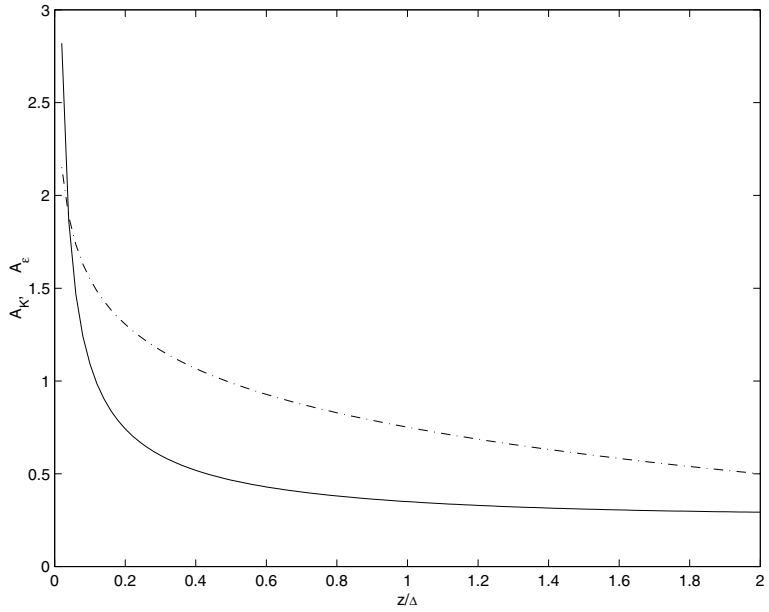

Figure 4. Solid line (——): A_K; dot-dashed line (– . – . –): A_ε.

viscous scale is $z_* = \nu/u_* \approx 0.2$ mm and the roughness length z_0 ranges from 0.01 to 1 m. However, a generalisation of the calculation made here to the simulation of flows at the scale of the laboratory is likely to be erroneous.

4. Solution

The previous spectral analysis based on the existence of a k_1^{-1} range in the energy spectrum indicates that the dissipation and diffusion processes should be modified in the subgrid models. The subgrid-scale lengths should be thus taken larger than the commonly used Prandtl length κz. In the present section, an approach is proposed to match the usual subgrid turbulence scheme and the similarity laws through the use of adequate expressions of subgrid-scale lengths near the surface. This approach is in agreement with the physical analysis given above and contrasts with the empirical modification of Smagorinsky constant as suggested by other authors.

4.1. NEUTRAL CASE

As discussed above, the subgrid-scale lengths are generally assumed to be equal to an effective grid mesh size. We propose here to determine these lengths to obtain a matching between the subgrid turbulence scheme and the similarity laws. Since

the basic hypothesis of subgrid turbulence schemes concerning isotropy is violated near the surface, we argue that the length L does not correspond to real scales of dissipation and mixing near the surface any more. The spectral calculations of Section 3 showed the following behaviour of the length scales

$$L_\varepsilon = A_\varepsilon z, \tag{40}$$

$$L_K = A_K z, \tag{41}$$

where $\mathcal{L}_\mathcal{K} = C_K L_K$ and $\mathcal{L}_\varepsilon = \frac{L_\varepsilon}{C_\varepsilon}$, C_K and C_ε being kept equal to their free-stream values given by Equations (8) and (9).

Using the results of Section 2, the similarity laws (Equations (14) and (15)), are exactly derived from the subgrid scheme by using the same value of constants C_ε and C_K both in the surface layer and the free-stress layer. The constants A_ε and A_K are then given by:

$$A_\varepsilon = \alpha^{3/2}\kappa C_\varepsilon \tag{42}$$

$$A_K = \frac{1}{\alpha^{1/2}}\frac{\kappa}{C_K}. \tag{43}$$

With $\alpha = 3.75$ (Wyngaard et al., 1974), A_ε and A_K are equal to 2.03 and 3.13 respectively. For $\alpha = 4.63$, we have $A_\varepsilon = A_K = 2.79$ (which is of the same order as the estimates given from the spectral considerations in Section 3). This value of α is close to the evaluation of various observational estimates and is in particular close to the value of 4.75 given in Stull (1988). Thus it seems reasonable to use this value as the proposed solution leading to a single value of subgrid-scale length $L = A_K z = A_\varepsilon z$ near the surface (this greatly simplifies the adaptation of pre-existing models to our new formulation).

This solution is very simple to implement for the neutral case in a model, as opposed to other solutions previously proposed in the literature. In the next section, due to this simplicity it is easily extended to any stability conditions.

4.2. General case

Assuming the stationary equilibrium for the turbulent kinetic energy and neglecting the turbulent transport, the turbulent kinetic energy in 1D reads:

$$-\overline{u'w'}\frac{\partial \overline{u}}{\partial z} - \overline{v'w'}\frac{\partial \overline{v}}{\partial z} + \frac{g}{\theta_r}\overline{w'\theta'} - \varepsilon = 0. \tag{44}$$

This equation simply expresses the equilibrium between shear production, buoyancy production and dissipation ε.

4.2.1. *Subgrid Scheme in Free-Stream Turbulence*

Expressions of various turbulent quantities shown here are those used in the Meso-NH model and presented in Cuxart et al. (2000). These expressions can be

considered as a generalisation of those previously given for the neutral case. They are also representative of subgrid schemes existing in most current models. The Reynolds stresses are modelled as previously by Equations (2), (3), and (4), though the turbulent kinetic energy E and the final expression of diffusion coefficient will be different.

The buoyancy flux reads as

$$-\overline{w'\theta'} = K_h \frac{\partial \overline{\theta}}{\partial z}. \tag{45}$$

In this expression, K_h is the eddy coefficient for the potential temperature and is given (Cuxart et al., 2000) as

$$K_h = C_H L_K E^{1/2} \phi_3(R_\theta), \tag{46}$$

$$\phi_3 = \frac{1}{1 + \frac{C_H}{C_\theta} \frac{g}{\theta_r} \frac{L_\varepsilon L_K}{E} \frac{\partial \overline{\theta}}{\partial z}}. \tag{47}$$

As for C_K and C_ε, the constants C_H and C_θ originate from the closure terms used to determine the turbulent fluxes from the second-order moment equations (Sommeria, 1976; Schmidt and Schumann, 1989). Thus it is possible to show (Schmidt and Schumann, 1989) that

$$2C_\theta = \pi \frac{4}{3\beta_3} \left(\frac{2}{3\alpha_3} \right)^{\frac{1}{2}}, \tag{48}$$

$$C_H = \frac{1}{\pi} \frac{4}{3\beta_3} \left(\frac{2}{3\alpha_3} \right)^{\frac{1}{2}}, \tag{49}$$

where β_3 is the 'three-dimensional' Corrsin constant. Measurements give $\beta_3 = 1.34 \pm 0.02$ (Andreas, 1987).

In the present model, the values of C_θ and C_H are 1.2 and 1.66, respectively.

Using Equations (2), (3), (5), (44), (45) and (46) after some algebra, the turbulent kinetic energy E, the momentum and heat fluxes read as:

$$E = \mathcal{L}_\varepsilon \mathcal{L}_\mathcal{K} \left[\left(\frac{\partial \overline{u}}{\partial z} \right)^2 + \left(\frac{\partial \overline{v}}{\partial z} \right)^2 \right] f(\mathrm{Ri}), \tag{50}$$

$$\overline{u'w'}^2 + \overline{v'w'}^2 = \mathcal{L}_\mathcal{K}{}^3 \mathcal{L}_\varepsilon \left[\left(\frac{\partial \overline{u}}{\partial z} \right)^2 + \left(\frac{\partial \overline{v}}{\partial z} \right)^2 \right]^2 f(\mathrm{Ri}), \tag{51}$$

$$-\overline{w'\theta'} = C_3 \mathcal{L}_\mathcal{K}{}^{3/2} \mathcal{L}_\varepsilon{}^{1/2} \left(\frac{\partial \overline{\theta}}{\partial z} \right) \left[\left(\frac{\partial \overline{u}}{\partial z} \right)^2 + \left(\frac{\partial \overline{v}}{\partial z} \right)^2 \right]^{1/2} \phi_3(\mathrm{Ri}) f(\mathrm{Ri})^{1/2}, \tag{52}$$

where

$$\mathrm{Ri} = \frac{g}{\theta_r} \frac{\dfrac{\partial \overline{\theta}}{\partial z}}{\left(\dfrac{\partial \overline{u}}{\partial z}\right)^2 + \left(\dfrac{\partial \overline{v}}{\partial z}\right)^2}, \tag{53}$$

$$f(\mathrm{Ri}) = 0.5\left(1 - (C_3 + C_4)\mathrm{Ri} + \sqrt{\left((1 - (C_3 + C_4)\mathrm{Ri})^2 + 4C_4\mathrm{Ri}\right)}\right), \tag{54}$$

$$\phi_3(\mathrm{Ri}) = \frac{1}{1 + \dfrac{C_4\mathrm{Ri}}{f(\mathrm{Ri})}}, \tag{55}$$

with $C_3 = \dfrac{C_H}{C_K}$ and $C_4 = \dfrac{C_H}{C_K}\dfrac{C_\varepsilon}{C_\theta}$.

It is worth noticing that the derivations above are general. In particular no assumption has been made about the surface layer, and no relationships such as similarity laws have been used. In the neutral case (Ri = 0 and $f(\mathrm{Ri}) = 1$), Equations (50) and (51) are identical to those derived in Section 2 (Equations (10) and (11)).

4.2.2. *Similarity Laws*

The Monin–Obukhov similarity theory for the surface layer allows us to relate the wind speed and temperature gradients to the friction velocity u_* and temperature scale T_*, respectively. In the general case, they depend on stability functions ϕ_m and ϕ_h, which represent non-dimensional gradients of wind shear and temperature, respectively:

$$\left[\left(\frac{\partial \overline{u}}{\partial z}\right)^2 + \left(\frac{\partial \overline{v}}{\partial z}\right)^2\right]^{\frac{1}{2}} = \frac{u_*}{\kappa z}\phi_m\left(\frac{z}{L}\right), \tag{56}$$

$$\frac{\partial \overline{\theta}}{\partial z} = \frac{T_*}{\kappa z}\phi_h\left(\frac{z}{L}\right), \tag{57}$$

$$L = -\frac{{u_*}^3}{\kappa \dfrac{g}{\theta_r} Q_s}, \tag{58}$$

$$w_* = \left(\frac{g}{\theta_r} Q_s z_i\right)^{1/3}, \tag{59}$$

$$Q_s = -u_* T_*, \tag{60}$$

where L is the Obukhov length scale, w_* the free convection velocity (Deardorff, 1970), z_i the height of inversion and Q_s the surface temperature flux.

The non-dimensional wind shear and temperature gradients are chosen as (Businger et al., 1971; Wyngaard and Coté, 1974):

$$\begin{cases} \phi_m &= (1 - 15\frac{z}{L})^{-\frac{1}{4}} \\ \phi_h &= 0.74(1 - 9\frac{z}{L})^{-\frac{1}{2}} \end{cases} \quad \text{for unstable case,} \tag{61}$$

$$\begin{cases} \phi_m &= 1 + 4.7\frac{z}{L} \\ \phi_h &= 0.74 + 4.7\frac{z}{L} \end{cases} \quad \text{for stable case.} \tag{62}$$

The expression for turbulent kinetic energy given in the neutral case (Equation (13)) can be extended to all stability conditions (Wyngaard and Coté, 1974; Redelsperger and Sommeria, 1981):

$$E = \begin{cases} \left(\alpha + (-\frac{z}{L})^{2/3}\right) {u_*}^2 + \beta {w_*}^2 & \text{for unstable case} \\ \alpha {u_*}^2 & \text{for stable case,} \end{cases} \tag{63}$$

where $\beta = 0.2$.

Using Equations (56) and (60), this expression can be written as

$$E = \alpha\, k^2 z^2 \left[\left(\frac{\partial \overline{u}}{\partial z} \right)^2 + \left(\frac{\partial \overline{v}}{\partial z} \right)^2 \right] \phi_E \left(\frac{z}{L}, \frac{z_i}{L} \right), \tag{64}$$

where

$$\phi_E = \begin{cases} \left[1 + \frac{1}{\alpha}(-\frac{z}{L})^{2/3} + \frac{\beta}{\alpha\, \kappa^{2/3}}(-\frac{z_i}{L})^{2/3} \right] \frac{1}{{\phi_m}^2} & \text{for unstable case} \\ \frac{1}{{\phi_m}^2} & \text{for stable case.} \end{cases} \tag{65}$$

The energy dissipation rate can be also scaled as

$$\frac{\kappa z}{{u_*}^3} \varepsilon = \phi_\varepsilon \left(\frac{z}{L} \right). \tag{66}$$

Nevertheless, no consensus exists on the form of ϕ_ε. Frenzen and Vogel (1992) give the following expression estimated by considering the energy budget:

$$\phi_\varepsilon = \phi_m - \frac{z}{L} - 0.16 \quad \text{for the unstable case,} \tag{67}$$

whereas, based on more direct measurement, Wyngaard et al. (1971) proposed

$$\phi_\varepsilon = \begin{cases} \left(1 + 0.5(-\frac{z}{L})^{2/3}\right)^{3/2} & \text{for unstable case} \\ 1 + 5\frac{z}{L} & \text{for stable case.} \end{cases} \tag{68}$$

4.2.3. *Solution*

As previously for the neutral case, we stipulate that the subgrid turbulence scheme and the similarity theory match in the surface layer. On the one hand, the subgrid turbulent fluxes are given as functions of Richardson number, Ri. On the other hand, the Monin–Obukhov fluxes are given as functions of the stability parameters $\frac{z}{L}$ and $\frac{z_i}{L}$. Using Equations (53) and (58), the Richardson number, Ri, can be related to $\frac{z}{L}$

$$\mathrm{Ri} = \frac{z}{L}\frac{\phi_h}{{\phi_m}^2}. \tag{69}$$

Using this relation, expressions for L_K and L_ε are obtained :

$$\mathcal{L}_\mathcal{K} = C_K L_K = \frac{\kappa z}{\alpha^{\frac{1}{2}}}\frac{1}{{\phi_m}^2\,{\phi_E}^{\frac{1}{2}}}, \tag{70}$$

$$\mathcal{L}_\varepsilon = \frac{L_\varepsilon}{C_\varepsilon} = \kappa z\,\alpha^{3/2}\frac{{\phi_E}^{\frac{3}{2}}\,{\phi_m}^2}{f}. \tag{71}$$

For the neutral case, it has been shown that to match the similarity theory and the subgrid turbulence scheme it was necessary to use the subgrid-scale lengths defined as $L_\varepsilon = L_K = Az$, where $A = \alpha^{3/2}\kappa C_\varepsilon = \frac{1}{\alpha^{1/2}}\frac{\kappa}{C_K} = 2.79$.

More generally, the subgrid-scale lengths can be defined as

$$L_K = Az\phi_L\left(\frac{z}{L}, \frac{z_i}{L}\right), \tag{72}$$

$$L_\varepsilon = Az\psi_L\left(\frac{z}{L}, \frac{z_i}{L}\right), \tag{73}$$

where ϕ_L and ψ_L are two stability functions defined as:

$$\phi_L = \frac{1}{{\phi_m}^2\,{\phi_E}^{\frac{1}{2}}}, \tag{74}$$

$$\psi_L = \frac{{\phi_E}^{\frac{3}{2}}\,{\phi_m}^2}{f}. \tag{75}$$

In the neutral case ($L = \infty$, Ri = 0, $\phi_m = f = 1$), $\phi_L = \psi_L = 1$. Before implementing this method in a numerical model, these expressions can be simplified. Two potential difficulties are the dependency on the inversion height z_i and the complicated function f. Figures 5a and 5b show the functions ϕ_L and ψ_L for various values of $\frac{z_i}{L}$. Both functions are clearly less dependent on $\frac{z_i}{L}$ than on $\frac{z}{L}$. This it seems acceptable to neglect the dependency on z_i when applying the relationships in the surface layer. On the other hand, it seems important to keep the dependency on the Obukhov length. To simplify the computation of the two new

functions, it is interesting to look at their ratio (Figure 6). As for the neutral case, the subgrid-scale lengths L_ε and L_K are identical. The plotted ratio of the functions also corresponds to the ratio of the subgrid-scale lengths. In the stable case, this ratio varies little. In the unstable case, the ratio increases from 1 to around 3 for $\frac{z}{L} = -1$. As shown on the same figure, a good approximation is given by:

$$\frac{\phi_L}{\psi_L} = \begin{cases} 1 - 1.9\frac{z}{L} & \text{for unstable case} \\ 1 - 0.3(\frac{z}{L})^{1/2} & \text{for stable case.} \end{cases} \tag{76}$$

Equations (74) and (76) lead to an equation system simple to implement in a model. This scheme has been used to obtain results presented in the following section, where it is referenced as the new subgrid scheme.

Stability functions for momentum, temperature and turbulent kinetic energy as deduced from this new scheme can be compared with the Monin–Obukov profiles as well as with the standard subgrid scheme with subgrid-scale lengths equal to κz or the mesh size Δ as usual in LES models. Figure 7 clearly shows the improvements brought by the new scheme over the usual methods. The use of κz for subgrid-scale lengths leads to an overestimate of the Values of the vertical gradients of momentum and potential temperature and the dissipation. The use of the mesh size leads to better results for unstable conditions, though still overestimating the momentum gradient and the dissipation by a factor of around 2.

4.2.4. *Matching with the Free-Stream Layer*

The developments described above allows one to reconcile the standard subgrid turbulence schemes and the similarity theory in the surface layer. Nevertheless, it is desirable that the standard behaviour of subgrid turbulence scheme is recovered in the regions away from the surface layer. As outlined above, the only difference concerns the specification of subgrid-scale lengths. In LES of free-stream turbulence, the lengths are generally assumed to be equal to the effective grid mesh size, as explained in Section 2.

To allow an implicit choice of the right length, a simple linear combination is proposed:

$$L_K = (1 - \gamma) A z \phi_L + \gamma \Delta \tag{77}$$

$$L_\varepsilon = (1 - \gamma) A z \psi_L + \gamma \Delta \tag{78}$$

where Δ is an average grid mesh spacing and γ a factor varying between 0 and 1 and controlling the transition of subgrid terms between the surface layer and the free atmosphere.

Such a γ factor was also introduced by SWM94 to ensure the transition of their formulations of subgrid momentum fluxes between the two layers. They choose to define this factor as the ratio of small- and large-scale strain rates. Their factor is only a function of z for a given simulation but presents the interesting feature that γ

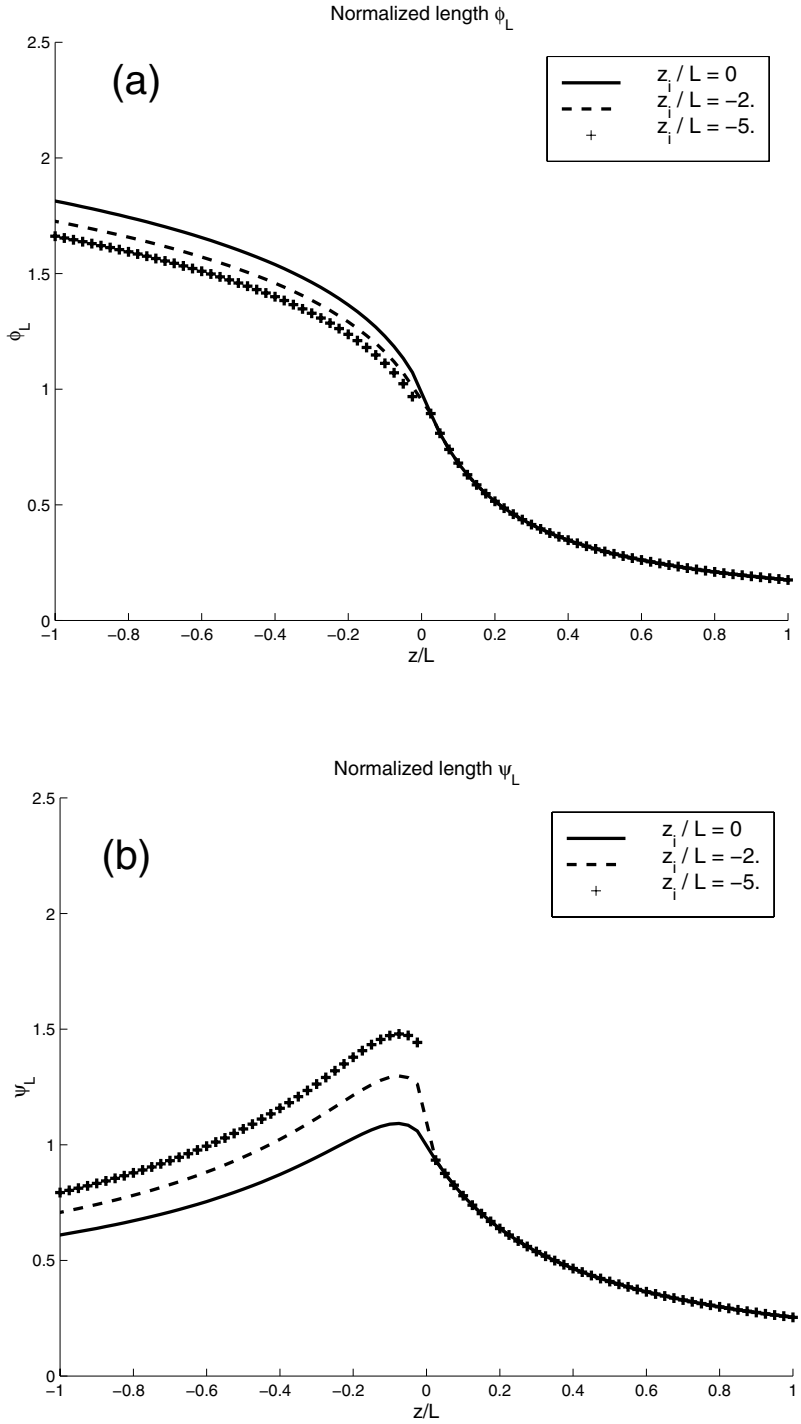

Figure 5. Normalized subgrid-scale lengths: (a) ϕ_L (Equation (74)) and (b) ψ_L (Equation (75)) as function of stability parameter z/L and for different values of z_i/L (-5, -2, 0).

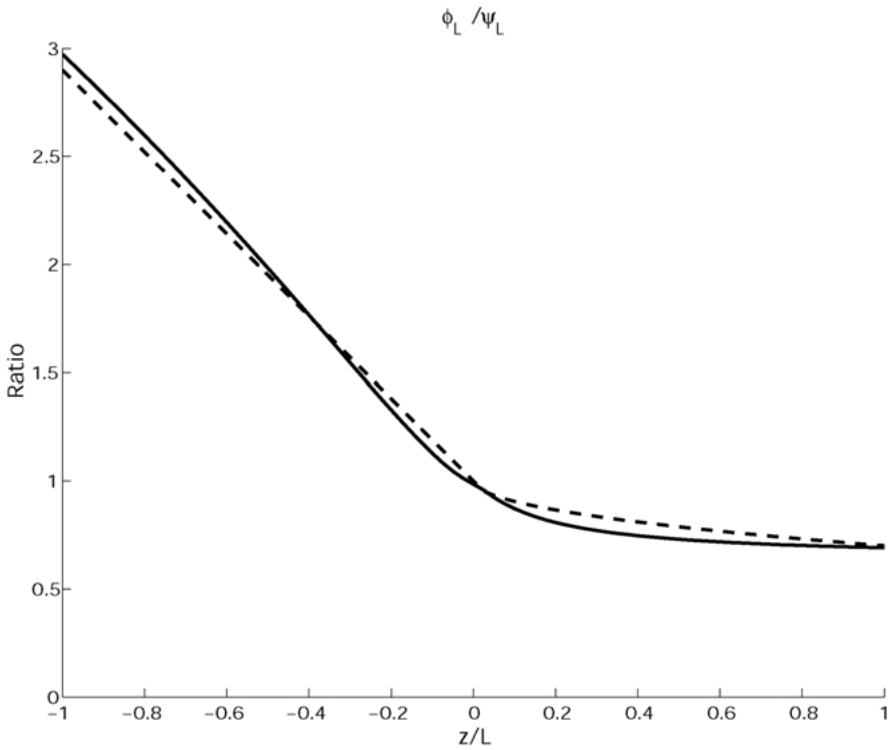

Figure 6. Ratio of subgrid scale-lengths as function of stability parameter z/L: exact equation (solid line) and approximated by Equation (76) (dashed line).

depends on the grid resolution. Indeed, it is expected that this factor increases with decreasing grid resolution as more small-scale eddies will be directly resolved by the model. As discussed above, one would like the present method to be simple to implement and suitable for LES models as well as mesoscale models and GCMs. In particular, it must be valid for any stability conditions and any surface conditions. Though the method of SWM94 does not seem to be easily applicable to inhomogeneous surface conditions, their numerical results are helpful in deriving a general expression for γ. Their results show in all cases an exponential increase of γ from 0 at the surface to 1 at a height $\frac{z}{3z_i}$. In the present case, we have chosen the following formulation, which roughly fits with the γ computed as the ratio of small- and large-scale strain rates in simulations of SWM94 as well as in the present ones:

$$\gamma = 1 - e^{-3\left(\frac{z_1 - z}{z_1 - z_c}\right)} \tag{79}$$

where z_1 is the height of the first level of subgrid fluxes computation in the model and z_c the height where $\gamma = 0.95$. The latter height depends on both horizontal and vertical model resolutions (Δ_x and Δ_z, respectively). Some heuristic arguments

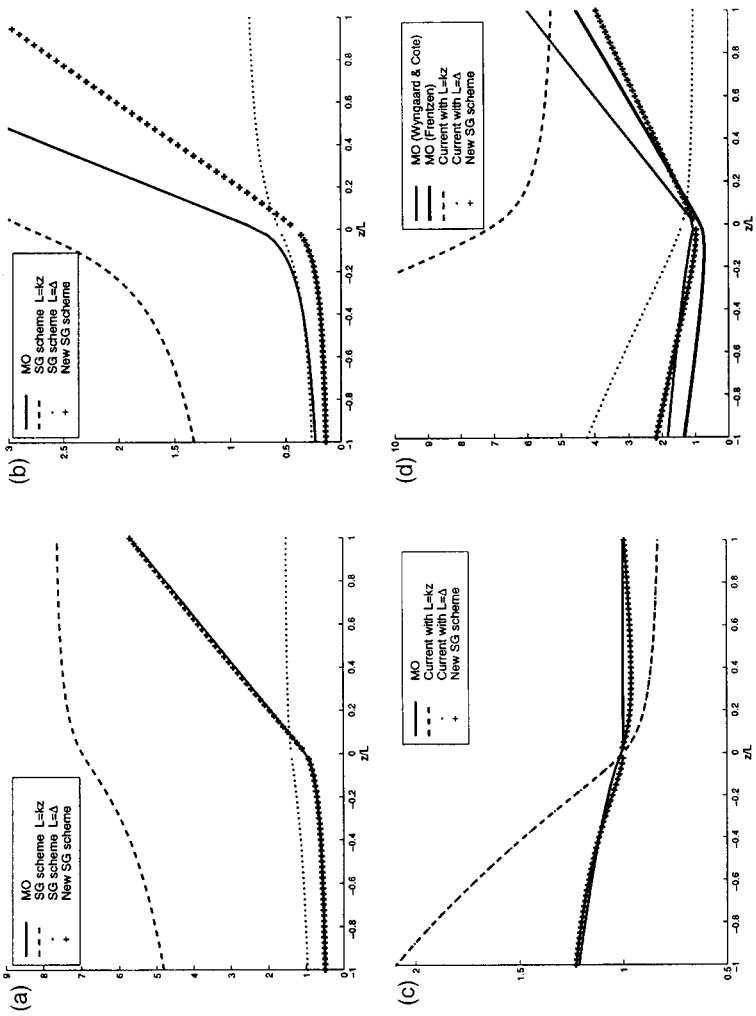

Figure 7. Theoretical profiles of stability function ϕ_m, ϕ_h, ϕ_E and ϕ_ε as function of z/L for momentum (a), potential temperature (b), turbulent kinetic energy (c) and energy dissipation (d), respectively. Curves are plotted for Monin–Obukov similarity law (solid line), standard subgrid turbulence scheme at the first half-level of model ($z = \frac{\Delta_z}{2}$ with L = κz (dashed line) and L = Δ_z (dotted line) and new scheme (plus).

can be developed to roughly estimate z_c, and depend on the knowledge of the size of energetic eddies in the surface layer, which are difficult to measure from observations (e.g., Counihan, 1975). Assuming that the vertical length of eddies is equal to κz and that the model is able to resolve the $2\Delta_z$ scales, z_c should be chosen larger than $\frac{2\Delta_z}{\kappa}$. The horizontal length of eddies can be estimated to be 1 to 3 times their vertical lengths, thus z_c should be chosen larger than $\frac{2\Delta_x}{3\kappa}$. Finally, this reasoning stands for the neutral case. For the unstable case, the vertical size of eddies is around $\frac{\kappa z}{\phi_m}$. On the basis of these simple arguments, the final expression for z_c is given by

$$z_c = \mathrm{Max}\left(\frac{2\Delta_z\phi_m}{\kappa}, \frac{2\Delta_x\phi_m}{3\kappa}\right). \tag{80}$$

In using results previously published as well as present simulations, these simple arguments seem to work. For example, an estimation of z_c from spectra obtained at different heights by Khana and Brasseur (1997) for a numerical experiment with horizontal and vertical mesh size of 20 and 1 m respectively, leads to a value of 40 m, close to the one obtained from Equation (79). For present numerical experiments, Figure 8 shows that similar variations of γ are obtained when using the Equation (79) or considering the ratio between the resolved flux and the total flux for u-momentum and potential temperature. The results show that the expression (79) works for the neutral case as well as for the convective case.

For mesoscale and large-scale models, another formulation of γ can be necessary and will be discussed in a forthcoming paper.

5. Results

5.1. Numerical model

The model used in present experiments is the LES (large-eddy simulation) version of the non-hydrostatic model, Meso-NH, presented for its dynamical part in Lafore et al. (1998). The 3D turbulence scheme is based on the scheme proposed by Redelsperger and Sommeria (1981, 1986) and is discussed in detail by Cuxart et al. (2000). It is based on a prognostic equation for subgrid kinetic energy and it incorporates the effect of thermal stratification on subgrid fluxes through variable Prandtl and Schmidt numbers.

We start the simulations from horizontally homogeneous conditions corresponding to a vertical profile. At the initial time, a random deviation of temperature with a maximum amplitude of 0.1 K is added at the first level of model, allowing a progressive development of eddies. No large-scale forcing is used in all simulations presented except a geostrophic wind taken into account through the Coriolis force ($f = 10^{-4}$ s^{-1}). A description of numerical experiments is given in Table I.

TABLE I

Description of numerical experiments. SGS stands for subgrid scheme of turbulence.

Experiment	Model							Atmosphere				
	SGS	Lx (km)	Ly (km)	Lz (km)	Δ_x (m)	Δ_z (m)	Nx × Ny × Nz	U_g (m s^{-1})	Q_0 (K m s^{-1})	z_0 (m)	z_i (km)	L (m)
NEUT-N	New	4	2	1.5	50	50	80 × 40 × 30	10		0.1		∞
NEUT-S	Standard	4	2	1.5	50	50	80 × 40 × 30	10		0.1		∞
CONV-N	New	5	5	2	50	50	100 × 100 × 40	15	0.06	0.16	1.1	−370
CONV-S	Standard	5	5	2	50	50	100 × 100 × 40	15	0.06	0.16	1.1	−370

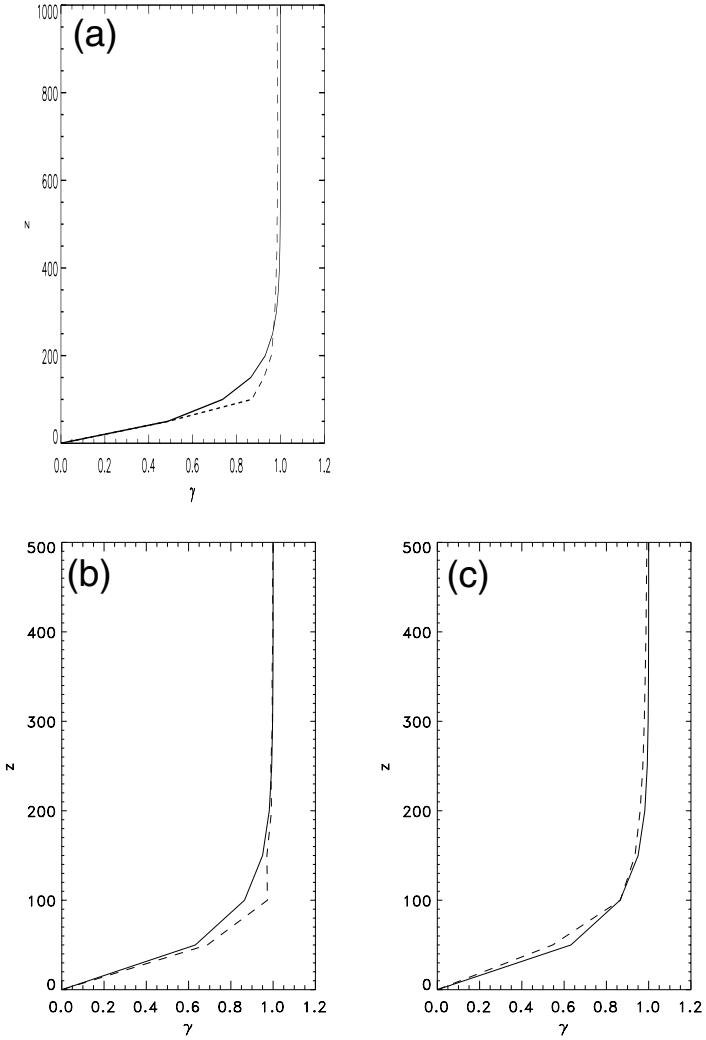

Figure 8. Factor γ (defined by Equation (78)) controlling the transition between the surface layer and the free atmosphere as given by the Equation (79) (solid lines) and as deduced from the ratio between the resolved flux and the total flux (dashed lines) for u-momentum (a) and (b) in the neutral and unstable case, respectively, and for vertical flux of temperature (c). Vertical axis is height in metres.

5.2. NEUTRAL CASE

The first case examined is a neutral case with main characteristics given on Table I. The model is run for 15 hours and the statistics made over the last 5 hours.

As the present paper focuses on the representation of the surface layer in LES, the numerical results are compared with the similarity theory, which is thus considered as the reference. The profiles are plotted in terms of dimensionless

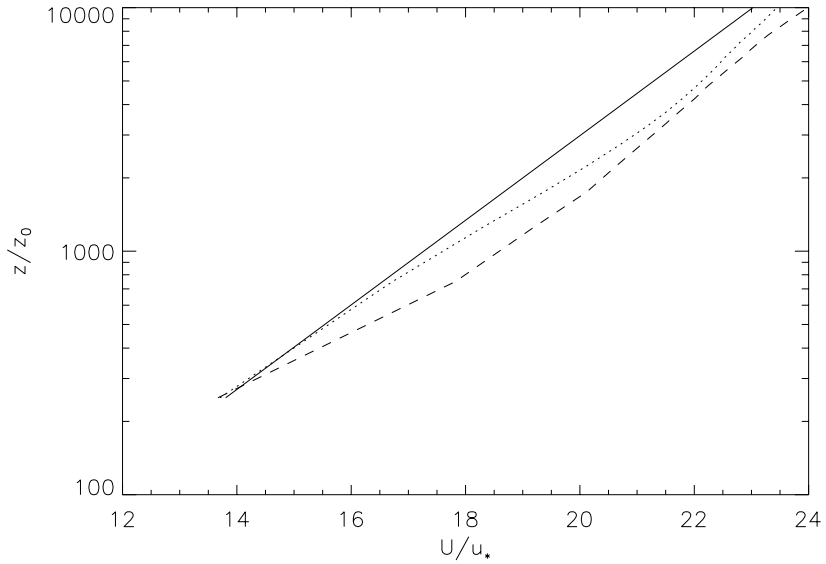

Figure 9. Wind speed profiles for the neutral case: as predicted by the similarity theory (solid line), as simulated with the standard (dashed line) and the new (dotted line) subgrid turbulence scheme.

coordinates z/z_0 and U/u_*, where the roughness length z_0 and the friction velocity u_* are equal to 0.1 m and 0.5 m s^{-1}, respectively. The experiment is performed two times, first with the standard subgrid scheme (NEUT-S) and second with the new scheme (NEUT-N) described in the previous sections of this paper.

The computed wind and vertical shear profiles are plotted in Figures 9 and 10, respectively. As expected, the wind profile shows improvements with the new scheme. Logarithmic velocity profile is only obtained with the standard scheme (NEUT-S) for the first model level. The new scheme (NEUT-N) allows us to successfully reproduce the logarithmic law up to $\frac{z}{z_0} = 1000$. A better agreement of LES with similarity theory is also observed for the shear (Figure 10) in the lowest levels, though overestimating the theoretical value.

Figure 11 shows the dissipation rate as normalized by ${u_*}^3$. The improvement in the surface layer with the new scheme is more spectacular than for momentum with a perfect agreement with the similarity law up to the height $2000\frac{z}{z_0}$.

5.3. UNSTABLE CASE

This second case considers the effect of stability on the behaviour of profiles in the surface layer. In order to evaluate the modifications of subgrid scheme in the surface layer, the conditions of the experiment are chosen to be similar to the main case studied by Khanna and Brasseur (1997) (hereafter KB97). Besides an improved subgrid scheme in the surface layer, KB97 also used a high resolution in the

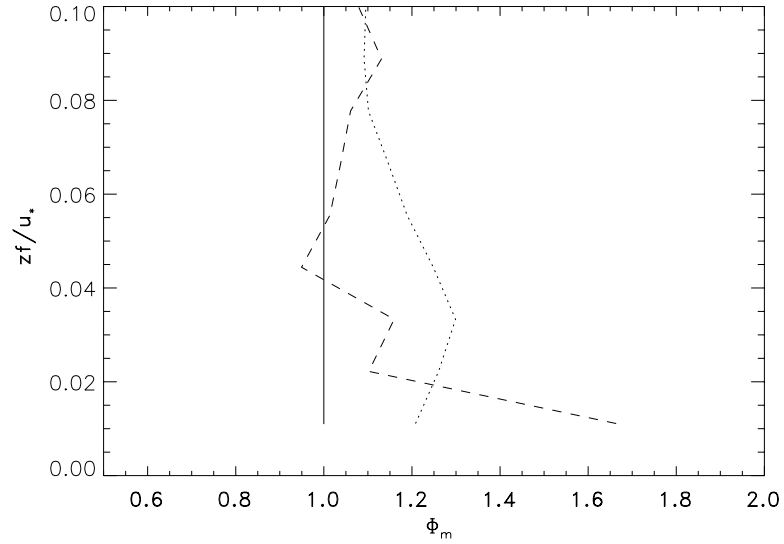

Figure 10. Momentum stability function profiles for the neutral case: as predicted by the similarity theory (solid line), as simulated with the standard (NEUT-S: dashed line) and the new (NEUT-N: dotted line) subgrid turbulence scheme.

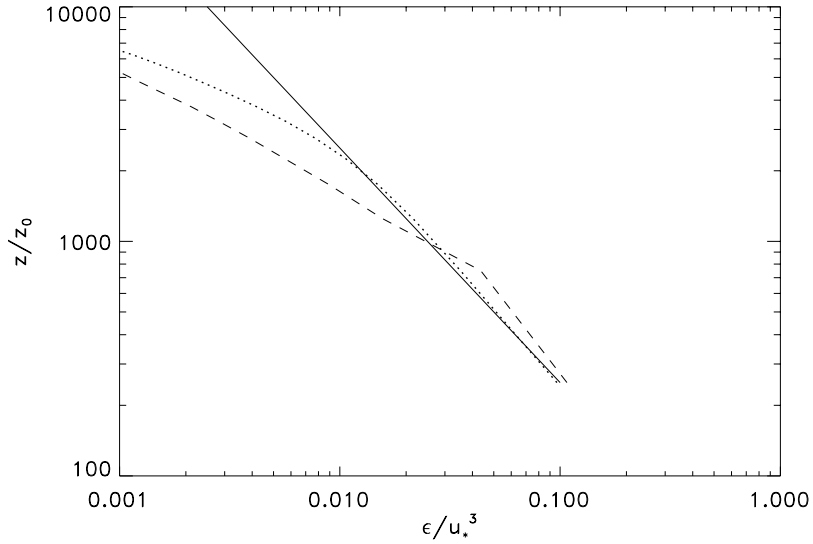

Figure 11. Profiles of dissipation rate scaled by ${u_*}^3$ for the neutral case in function of $\frac{z}{z_0}$: as predicted by the similarity theory (solid line), as simulated with the standard (NEUT-S: dashed line) and the new (NEUT-C: dotted line) subgrid turbulence scheme.

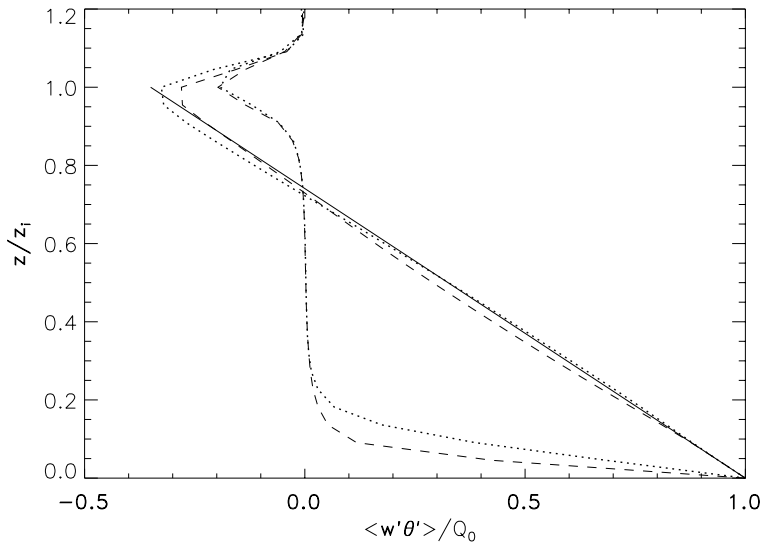

Figure 12. Vertical profile of the potential temperature flux for the unstable case as simulated with the standard (CONV-S: dashed line) and the new (CONV-N: dotted line) subgrid turbulence scheme. Subgrid fluxes are also representated.

surface layer, thanks to grid nesting techniques. The initial conditions correspond to a common case in the atmosphere, namely a convective boundary layer with shear (Table I). Though initial conditions and domain size are similar to KB97, the isotropic resolution used in the present experiment (mesh size 50 m) is much less than the one used by KB97 in the surface layer (mesh size 1 m) and therefore suitable for realistic computations. The present model is run with the standard and the new scheme (experiments CONV-S and CONV-N, respectively). It is first important to check that proposed modifications in the subgrid scheme do not cause the solution to deteriorate above the surface layer. Figure 12 shows that the vertical flux of potential temperature is almost unchanged though the subgrid part and the entrainment are slightly larger with the new scheme. The same conclusions hold for the vertical flux of horizontal momentum along the shear (Figure 13). In both cases, the total streamwise momentum vertical flux decreases roughly as predicted by similarity laws. As noted by Moeng and Sullivan (1994), the entrainment at the inversion leads to a departure from the standard similarity law, which does not take into account the presence of an inversion layer.

Changes brought about are expected to be more spectacular in the surface layer. To evaluate the results, profiles are compared to similarity laws (Businger et al., 1971) and KB97 numerical results. The run with the standard subgrid scheme (CONV-S) largely overpredicts the mean shear (Figure 14) and the vertical gradient of potential temperature (Figure 15) as estimated from the similarity laws.

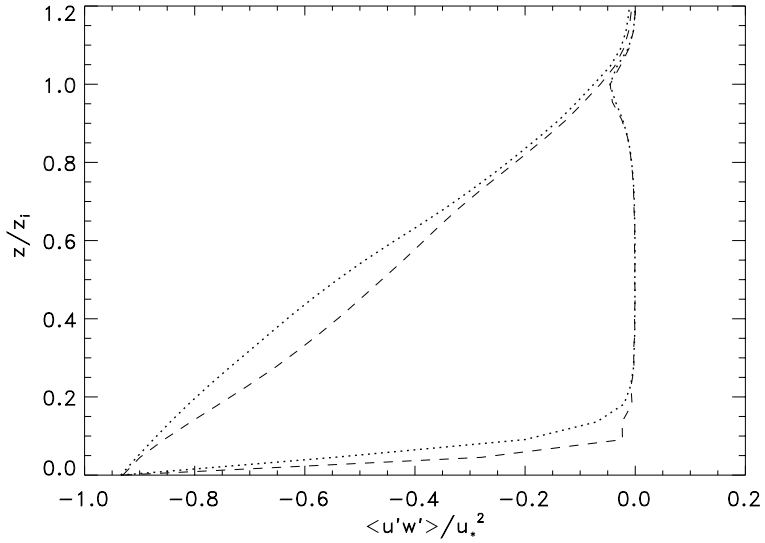

Figure 13. Vertical profile of the along-wind momentum flux for the unstable case: as predicted by the similarity theory (solid line), as simulated with the standard (CONV-S: dashed line) and the new (CONV-N: dotted line) subgrid turbulence scheme. Subgrid fluxes are also plotted.

Moreover, spurious vertical oscillations of the shear profile are obtained in the low levels and are probably a consequence of the overestimated shear predicted at the first model level. The new subgrid scheme allows clear improvement for both quantities and is in reasonable agreement with the KB97 results obtained with at once a subgrid scheme modified in the surface layer following SWM94 and a much higher resolution than presently. Figure 16 shows the dissipation rate of turbulent kinetic energy, it scales rather well with $\frac{kz}{u_*}$ as given by the Monin–Obukhov theory. A decrease with height is obtained up to $\frac{z}{L} = -0.3$ with the new subgrid scheme as predicted by the similarity theory. Above this height, where one can be considered to be above the surface layer, a decrease is found in the simulation, in contrast to the similarity laws. This region can be considered as a transition region from surface-layer to mixed-layer scalings (e.g., Moeng and Sullivan, 1994; KB97).

6. Conclusion

To represent both the surface-layer and free-stream turbulence with a unique parameterization is a difficulty in all numerical atmospheric models, even in LES. This paper has provided a physical explanation and a general solution suitable for any atmospheric models, including inhomogeneous surface conditions, complex topography and any vertical stability. The energy deficit of blocked turbulence for a given dissipation has been shown to have a dramatic effect on the mixing

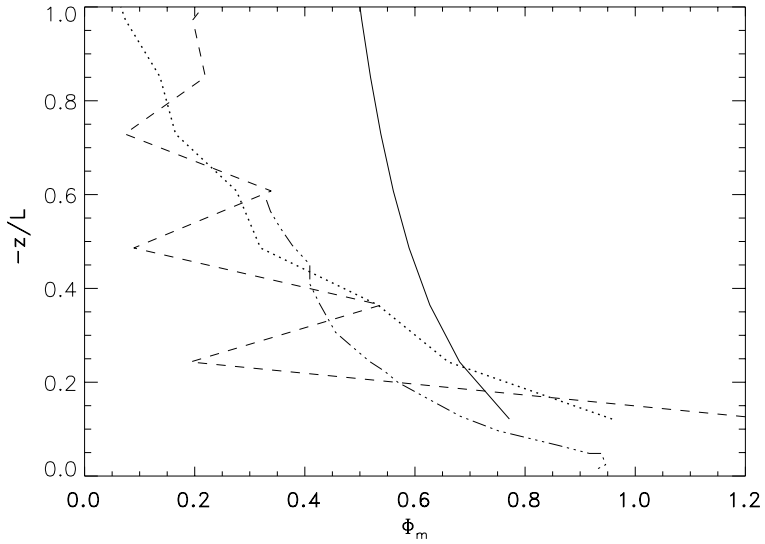

Figure 14. Momentum stability function (ϕ_m) profiles for the unstable case: as predicted by the similarity theory (solid line), as simulated with the standard (CONV-S: dashed line) and the new (CONV-N: dotted line) subgrid turbulence scheme. Dashed-dotted line reproduces the result of KB97 for same case.

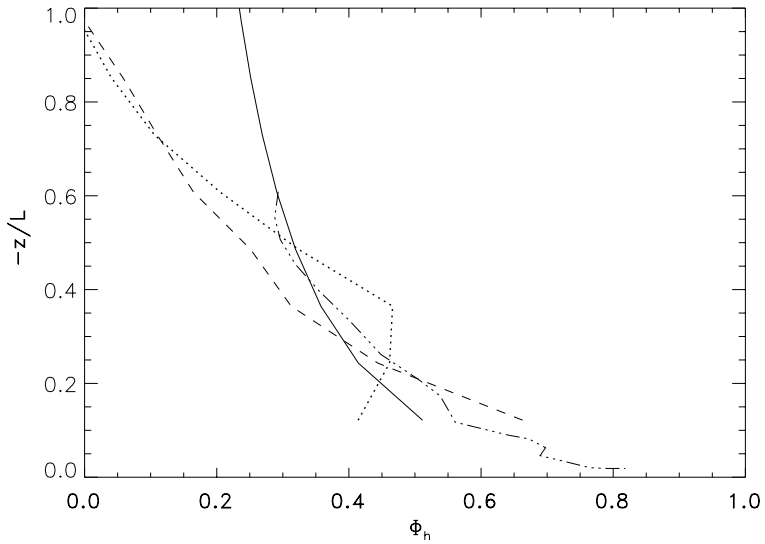

Figure 15. Potential temperature stability function (ϕ_h) profiles for the unstable case: as predicted by the similarity theory (solid line), as simulated with the standard (CONV-S: dashed line) and the new (CONV-N: dotted line) subgrid turbulence scheme. Dashed-dotted line reproduces the result of KB97 for same case.

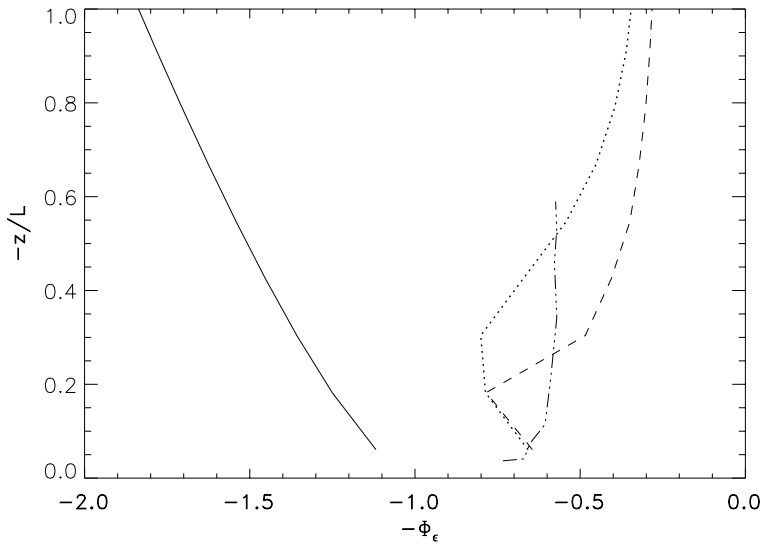

Figure 16. Dissipation rate function profiles for the unstable case: as predicted by the similarity theory (solid line), as simulated with the standard (CONV-S: dashed line) and the new (CONV-N: dotted line) subgrid turbulence scheme. Dashed-dotted line reproduces the result of KB97 for same case.

and dissipation lengths to be used in subgrid models close to the ground. To take into account this 'anomalous dissipation', modifications in the standard subgrid schemes derived for free-stream turbulence have been proposed. These modifications are simple to implement in models and are physically justified by recent measurements of spectra close to the ground. As described in a forthcoming paper, this method is also easily applicable to mesoscale and large-scale models. This is considered as an improvement over more empirical methods based on an increase of the Smagorinsky coefficient (e.g., Mason, 1989; Mason and Thomson, 1992).

As shown for neutral and convective cases with wind shear, these changes in the subgrid turbulent scheme allow one to substantially improve the prediction of profiles of mean quantities in the surface layer. Agreement with similarity laws is found up to about $0.2z_i$, for simulated shear and stability profiles and dissipation rates of turbulent kinetic energy.

Clearly, the modifications proposed are only a first step to improve LES results in the surface layer. They have the great advantage of being applicable to any numerical models and of being very easily implemented. They provide an alternative to the use of large coefficients used in some boundary-layer schemes implemented in global climate models. As suggested recently by Juneja and Brasseur (1999), the basic hypothesis used in the LES models need probably to be reconsider when applied to study the surface layer. Moreover the physical mechanism of dissipation is strongly modified by the presence of the ground (cf. Hunt and Carlotti, 2000).

The present article presents the immediate and practical consequences of these ideas on subgrid models. The next step should be a deeper modification of subgrid models with regards to these new concepts.

Acknowledgements

We would like to thank our different institutions CNRS, CNRM, DAMTP and ONERA that have facilitated this work. We are very grateful for the help of P. Jabouille and I. Mallet who helped us to install the model on ONERA supercomputers. Initial discussions with Ph. Bougeault, J. C. R. Hunt, J. Stein and N. Wood helped to develop some of the ideas presented in this paper. We would also like to thank Matthew M. Scase helped us with language improvements in the final version.

References

Andreas, E. L.: 1987, 'On the Kolmogorov Constants for the Temperature-Humidity Cospectrum and the Refractive Index Spectrum', *J. Atmos. Sci.* **44**, 2399–2406.

Andrén, Brown, A. R., Graf, J., Mason, P. J., Moeng, C., Nieuwstadt, F. T. M., and Schumann U.: 1994, 'Large-Eddy Simulation of a Neutrally Stratified Boundary Layer: A Comparison of Four Computer Codes', *Quart. J. Roy. Meteorol. Soc.* **120**, 1457–1484.

Businger, J. A., Wyngaard, J. C., Izumi, Y., and Bradley, E. F.: 1971, 'Flux-Profile Relationships in the Atmospheric Surface Layer', *J. Atmos. Sci. Sci.* **28**, 181–189.

Caughey, S. J. and Palmer, S. G.: 1979, 'Some Aspects of Turbulence Structure through the Depth of the Convective Boundary Layer', *Quart. J. Roy. Meteorol. Soc.* **105**, 811–827.

Counihan, J.: 1975, 'Adiabatic Atmospheric Boundary Layers: A Review and Analysis of Data from the Period 1880–1972', *Atmos. Environ.* **9**, 871–905.

Cuxart, J., Bougeault, Ph., and Redelsperger, J. L.: 2000, 'A Multiscale Turbulence Scheme Apt for LES and Mesoscale Modelling', *Quart. J. Roy. Meteorol. Soc.* **126**, 1–30.

Deardorff, J. W.: 1970, 'Convective Velocity and Temperature Scales for the Unstable Planetary Boundary Layer and for Rayleigh Convection', *J. Atmos. Sci.* **27**, 1211–1213.

Frenzen, P. and Vogel, C. A.: 1992, 'The Turbulent Kinetic Energy Budget in the Atmospheric Surface Layer: A Review and an Experimental Reexamination in the Field', *Boundary-Layer Meteorol.* **60**, 49–76.

Fuerher, P. L. and Friehe, C. A.: 1999, 'A Physically Based Turbulent Velocity Time Series Decomposition', *Boundary-Layer Meteorol.* **90**, 241–295.

Garratt, J. R.: 1992, *The Atmospheric Boundary Layer*, Cambridge University Press, Cambridge, 316 pp.

Hoxey, R. P. and Richards, P. J.: 1992, 'Spectral Characteristics of the Atmospheric Boundary Layer near the Ground', in *1st UK Wind Engineering Conference*, Cambridge.

Hunt, J. C. R. and Carlotti, P.: 2001, 'Statistical Structure of the High Reynolds Number Boundary Layer', *Flow Turbul. Combust.*, in press.

Hunt, J. C. R. and Morrison, J. F.: 2000, 'Eddy Structure in Turbulent Boundary Layers', *Eur. J. Mech., B Fluids* **19**, 673–694.

Juneja, A. and Brasseur, J. G.: 1999, 'Characteristics of Subgrid-Resolved-Scale Dynamics in Anisotropic Turbulence, with Application to Rough-Wall Boundary Layers', *Phys. Fluids* **11**, 3054–3067.

Khanna, S. and Brasseur, J. G.: 1997, 'Analysis of Monin–Obukhov Similarity from Large-Eddy Simulation, *J. Atmos. Sci.* **345**, 251–286.

Khanna, S. and Brasseur, J. G.: 1998, 'Three-Dimensional Buoyancy- and Shear-Induced Local Structure of the Atmospheric Boundary Layer', *J. Atmos. Sci.* **55**, 710–743.

Kim, K. C. and Adrian, R. J.: 1999, 'Very Large Scale Motion in the Outer Layer', *Phys. Fluids* **11**, 417–422.

Lafore, J. P., Stein, J., Asencio, N., Bougeault, P., Ducrocq, V., Duron, J., Fisher, C., Hereil, P., Mascart, P., Pinty, J. P., Redelsperger, J. L., Richard, E., and Vila-Guerau de Arellano, J.: 1998, 'The Meso-NH Atmospheric Simulation System. Part I: Adiabatic Formulation and Control Simulations', *Ann. Geophys.* **16**, 90–109.

Louis, J. F.: 1979, 'A Parametric Model of Vertical Eddy Fluxes in the Atmosphere', *Boundary-Layer Meteorol.* **17**, 187–202.

Mason, P. J.: 1989, 'Large-Eddy Simulation of the Convective Atmospheric Boundary Layer', *J. Atmos. Sci.* **46**, 1492–1516.

Mason, P. J. and Thomson, D. J.: 1992, 'Stochastic Backscatter in Large-Eddy Simulations of Boundary Layers', *J. Fluid Mech.* **242**, 51–78.

Moeng, C. H. and Sullivan, P. P.: 1994, 'A Comparison of Shear- and Buoyancy-Driven Planetary Boundary Layer Flows', *J. Atmos. Sci.* **51**, 999–1022.

Moin, P. and Kim, J.: 1982, 'Numerical Investigation of Turbulent Channel Flow', *J. Fluid Mech.* **118**, 341–377.

Panofsky, H. A., Tennekes, H., Lenschow, D. H., and Wyngaard, J. C.: 1977, 'The Characteristics of Turbulent Velocity Components in the Surface Layer under Convective Conditions', *Boundary-Layer Meteorol.* **11**, 355–361.

Porté-Agel, F., Meneveau C., and Parlange, M. C.: 2000, 'A Scale-Dependent Dynamic Model for Large-Eddy Simulation: Application to a Neutral Atmospheric Boundary Layer', *J. Fluid. Mech.* **415**, 261–284.

Redelsperger, J. L. and Sommeria, G.: 1981, 'Méthode de représentation de la turbulence d'échelle inférieure à la maille pour un modèle tridimensionnel de convection nuageuse', *Boundary-Layer Meteorol.* **21**, 509–530.

Redelsperger, J. L. and Sommeria, G.: 1986, 'Three-Dimensional Simulation of a Convective Storm: Sensitivity Studies on Subgrid Parameterization and Spatial Resolution', *J. Atmos. Sci.* **43**, 2619–2635.

Schmidt, H. and Schumman, U.: 1989, 'Coherent Structure of the Convective Boundary Layer Derived from Large Eddy Simulations', *J. Fluid Mech.* **200**, 511–562.

Schumann U.: 1975, 'Subgrid Scale Model for Finite Difference Simulations of Turbulent Flows in Plane Channels and Annuli', *J. Comp. Phys.* **18**, 376–404.

Sommeria, G.: 1976, 'Three-Dimensional Simulation of Turbulent Processes in an Undisturbed Trade Wind Boundary Layer', *J. Atmos. Sci.* **33**, 216–241.

Stull, R.: 1988, *An Introduction to Boundary Layer Meteorology*, Kluwer Academic Publishers, Dordrecht, 666 pp.

Sullivan, P. P., McWilliams, J. C., and Moeng, C. H.: 1994, 'A Subgrid-Scale Model for Large-Eddy Simulation of Planetary Boundary-Layer Flows', *Boundary-Layer Meteorol.* **71**, 247–276.

Thérry, G. and Lacarrère, P.: 1983, 'Improving the Eddy Kinetic Energy Model for Planetary Boundary Layer Description', *Boundary-Layer Meteorol.* **25**, 63–68.

Townsend, A. A.: 1976, *The Structure of Turbulent Shear Flow*, Cambridge University Press, Cambridge, 429 pp.

Troen, I. and Mahrt, L.: 1986, 'A Simple Model of the Atmospheric Boundary-Layer: Sensitivity to Surface Evaporation', *Boundary-Layer Meteorol.* **37**, 129–148.

Wyngaard, J. C. and Coté, O. R.: 1974, 'The Evolution of a Convective Planetary Boundary Layer: A Higher Order Closure Model Study', *Boundary-Layer Meteorol.* **7**, 289–308.

Wyngaard, J. C., Coté, O. R., and Isumi, Y.: 1971, 'Local Free Convection, Similarity and the Budgets of Shear Stress and Heat Flux', *J. Atmos. Sci.* **28**, 1171–1182.